SEMARAK ILMU PUBLISHING

Journal of Advanced Research in Numerical Heat Transfer

Journal homepage:
https://semarakilmu.com.my/journals/index.php/arnht/index
ISSN: 2735-0142

Numerical Simulation on Flow and Heat Transfer Characteristics of a Single-loop Oscillating Heat Pipe with Variable Pipe Diameter Ratios

Lu Hongkun[1,2,#], Muhamad Mat Noor[2,3,4,*], Ning Shuigen[1,2], Kumaran Kadirgama[2]

[1] School of Automotive Engineering, Jiangxi Polytechnic University, Jiujiang 332000, Jiangxi, China
[2] Faculty of Mechanical & Automotive Engineering Technology, University Malaysia Pahang Al-Sultan Abdullah (UMPSA), Pekan, Pahang, Malaysia
[3] Centre for Research in Advanced Fluid & Processes, Universiti Malaysia Pahang Al-Sultan Abdul-lah, Pekan 26600, Malaysia
[4] Institute of Sustainable and Renewable Energy (ISuRE), Universiti Malaysia Sarawak (UNIMAS), 94300, Kota Samarahan, Sarawak, Malaysia

ARTICLE INFO

Article history:
Received 9 August 2024
Received in revised form 10 September 2024
Accepted 14 October 2024
Available online 30 November 2024

Keywords:
Oscillating heat pipe; Diameter ratio; Heat transfer; Multi-phase flow; VOF

ABSTRACT

A three-dimensional numerical model, employing the Volume of Fluid (VOF) method, was developed for a single-loop oscillating heat pipe (OHP) with variable diameters. The investigation explored the impact of varying pipe diameter ratios on flow and heat transfer characteristics at different operational stages under a 40W heat power. The results reveal that the diameter ratio significantly affects the spatial arrangement of the evaporation, adiabatic, and condensation sections in the OHP. In the initial stage, the condensation section displays 15 liquid slugs when the diameter ratio is 1, but this number decreases to fewer than 10 in the same area when the diameter ratio exceeds 1. Comparative to a straight-pipe OHP, configurations with varying diameter ratios exhibit a marginal reduction in the average fluid velocity during the circulation of the working fluid inside the pipe, with the most pronounced velocity decrease occurring at a diameter ratio of 0.8. As the diameter ratio increases to 1.25 and 1.5, the turbulent disturbances in the region where the working fluid flows from the adiabatic section to the evaporation or condensation section intensify, facilitating the temperature exchange within the OHP. During stable operation of the OHP, the frequency of temperature oscillations increases with an increasing diameter ratio, while the amplitude decreases. Among all the cases, the OHP with a diameter ratio of 1.25 has the optimal heat resistance, 1.50K/W. The heat transfer performance of the OHP with a pipe diameter ratio of 0.8 deteriorated, and the thermal resistance increased by 27.6% compared with the straight-pipe OHP.

1. Introduction

Thermal management is essential in both daily life and industrial production [1-3]. Among various thermal management techniques, heat pipes have garnered significant attention due to their superior thermal conductivity [4]. A relatively newer type, the oscillating heat pipe (OHP), also referred to as a pulsating heat pipe (PHP), was first introduced by Akachi in 1990 [5]. Compared to conventional heat pipes, OHP offers several notable advantages: it enables highly efficient heat

Corresponding author.
[#] *E-mail address: maxlhk@163.com (Lu Hongkun)*
[*] *E-mail address: muhamad@umpsa.edu.my (Muhamad Mat Noor)*

https://doi.org/10.37934/arnht.27.1.4565

transfer without requiring external mechanical power, consists solely of bent capillary tubes without a wick structure, and is characterized by their simplicity and cost-effectiveness. Furthermore, the OHP is available in various designs, exhibits strong adaptability to different environments, and possesses high heat transfer limits [6,7]. These characteristics make the OHP a promising solution for addressing overheating challenges across a broad range of applications [8]. Currently, OHPs are widely used in aerospace, high-heat-flux electronic devices [9], light-emitting diodes (LED) [10], solar photovoltaic systems [11], waste heat recovery [12], and heating, ventilation, and air conditioning (HVAC) systems [13]. Moreover, OHPs show significant potential in other areas, such as numerical control (NC) machine [14], the wheel conner module (WCM) [15] and battery thermal management system (BTMS) [16,17].

Research has shown that the factors influencing the thermal performance of OHPs can be categorized into three groups: geometric parameters, operating parameters, and physical parameters [18]. Among these, structural optimization of OHPs is fundamental to their widespread application [19]. To design and develop more stable and higher-performing OHP structures, it is crucial to gain a deeper understanding of the underlying operating mechanisms of OHP. The OHP achieves efficient heat transfer through the oscillatory movement of vapor and liquid slugs, driven by pressure imbalances between adjacent tubes [20]. This process involves a range of complex phenomena, including phase transitions of the working fluid, bubble growth and collapse, nucleate boiling, and forced convection [21]. With advancements in computational fluid dynamics (CFD) and the availability of greater computational power, CFD has emerged as a valuable tool for elucidating the intricate flow characteristics and heat transfer mechanisms within OHP [22].

At present, most applications based on OHPs use copper tubes with uniform diameters. Innovating the cross-sectional shape to develop OHPs with enhanced startup and heat transfer performance is crucial for advancing their practical use [23]. In simulation studies aimed at optimizing the cross-sectional shape of OHPs, the single-loop OHP is predominantly used. This approach is preferred for two key reasons. First, the single-loop OHP retains all the essential characteristics of a typical OHP, allowing its simulation results to be more easily compared and validated against Visualizing experimental data, thereby providing a solid basis for verifying numerical models. Second, simulating the transient operation of OHPs using computational fluid dynamics (CFD) involves multiphase flow and complex thermodynamic equations, which demand substantial computational resources and are prone to numerical instability [24]. By employing a single-loop OHP, researchers can more effectively control boundary conditions, minimizing potential issues with computational convergence [25].

In recent years, numerous researchers have demonstrated significant interest in optimizing the structure of single-loop OHPs [26]. Xie *et al.,* [27], through a two-dimensional (2D) numerical study, investigated the impact of different bend designs on the flow and heat transfer performance of single-loop closed OHPs. Their findings revealed that OHPs with right-angle bends exhibited faster startup times and superior heat transfer performance compared to those with circular bends. Wang *et al.,* [28] examined the startup and heat transfer performance of single-loop OHPs featuring one straight tube and another side tube with varying inner diameter ratios. Their research showed that at a heating power of 20W, the OHP with a 4:3 inner diameter ratio achieved the lowest thermal resistance and the highest heat transfer performance. Kang *et al.,* [29] introduced a novel single-loop OHP design with partition walls inside the flow channels and analyzed the effects of wall placement and filling ratio using a 2D numerical model. The results indicated that, with a 70% filling ratio, the OHP with partition walls improved thermal performance by 14%. Similarly, Zhao *et al.,* [30] conducted a 2D numerical study on single-loop OHPs equipped with wick structures, evaluating the influence of wick characteristics and filling ratios on thermal performance. Their results

demonstrated that at filling ratios of 50% and 70%, the working fluid in the OHP with wick structures exhibited mist-like flow, leading to enhanced performance. However, at a 30% filling ratio, the performance of the OHP with wick structures was inferior to that of a conventional single-loop OHP. Rasoul *et al.,* [31] designed and fabricated a three-diameter OHP (TD-OHP) to study its flow behavior and heat transfer performance. Their research demonstrated that the uneven diameters, which induce unbalanced gravitational forces, accelerated the generation, growth, and rupture of bubbles. Compared to single-diameter OHP (SD-OHP) and double-diameter OHP (DD-OHP) designs, the TD-OHP structure significantly enhanced circulation flow and reduced thermal resistance. Similarly, Chen *et al.,* [32] investigated the impact of varying inner diameters on the startup and operation of single-loop OHPs, comparing the performance of OHPs with inner diameters of 6 mm and 3 mm under different filling ratios and heating powers. Their study found that OHPs with a 6 mm inner diameter were more prone to forming excessively long liquid columns, resulting in intermittent pulsation. In contrast, the 3 mm inner diameter, with its enhanced surface tension, facilitated smoother liquid slug movement within the tube, preventing such pulsation. Liu *et al.,* [33] proposed three types of single-loop double-diameter OHPs (DOHPs) and evaluated their startup and heat transfer performance using 2D transient numerical simulations. Their results identified two bubble growth modes in the OHPs: directional growth and rapid coalescent growth. The variation in diameters significantly influenced DOHP performance, with the DPHP featuring a 2.0 mm diameter difference showing the best performance. Specifically, the startup time and thermal resistance were reduced by 19.1% and 34.5%, respectively.

In summary, existing studies have demonstrated that appropriately designed multi-diameter OHP structures can significantly enhance the heat transfer performance of OHPs. However, there are still some limitations in the current research. Firstly, most studies on multi-diameter OHPs rely on 2D transient numerical simulations, which may limit the accuracy in capturing complex phenomena such as phase changes and vortex formation. Secondly, no studies have yet explored the effect of varying pipe diameters along the evaporation/condensation and adiabatic sections of an OHP, transitioning from a tapered section to a straight tube and then to an expanded section. In this study, a three-dimensional (3D) transient numerical simulation will be conducted to investigate the flow and heat transfer characteristics of OHPs with varying diameters, utilizing the Volume of Fluid (VOF) method combined with the Lee phase-change model [34]. The analysis will focus on the effects of diameter ratio variations on the initial distribution of the working fluid, the startup process, steady-state flow behavior, and overall heat transfer capacity. The findings are expected to provide a certain insight for the future structural optimization designs of OHP-based systems.

2. Numerical Simulation Method

2.1 Control Equation

In this study, the VOF method is employed to track the vapor-liquid interface in the OHP. The VOF method is suitable for two or more immiscible fluids. Therefore, based on the volume fraction within a computational cell, the control volume can be categorized into two situations: one where a pure fluid is present (α_l=1), and the other where a mixed fluid is present ($\alpha_l \neq 1$). There are only two phases in the OHP: liquid and vapor. When the control volume contains either only the vapor phase or the liquid phase, the governing equations are identical to those of single-phase flow. However, in the presence of a phase interface within the control volume, the sum of the vapor and liquid phase volume fractions equals 1, as shown in Eq. (1).

$$\alpha_v + \alpha_l = 1 \tag{1}$$

The governing equations of flow and heat transfer are shown in Eqs. (2)-(5) [35].
Continuity equation:

$$\frac{\partial}{\partial t}(\alpha_l \rho_l) + \nabla \cdot (\alpha_l \rho_l v) = S_{m,l} \tag{2}$$

$$\frac{\partial}{\partial t}(\alpha_v \rho_v) + \nabla \cdot (\alpha_v \rho_v v) = S_{m,v} \tag{3}$$

$$\frac{\partial}{\partial t}(\rho v) + \nabla \cdot (pvv) = \nabla[\mu(\nabla v + \nabla v^T)] + \rho g + F \tag{4}$$

Energy conservation equation:

$$\frac{\partial}{\partial t}(\rho E) + \nabla[v(\rho E + p)] = \nabla \cdot (k \nabla T) + S_E \tag{5}$$

The velocity field and temperature field solved by the momentum equation and energy equation are shared by the vapor phase and liquid phase fluid [35], so the physical properties of the mixed phase are used in the momentum equation and energy equation, as shown in Eq. (6).

$$\rho = \alpha_l \rho_l + \alpha_v \rho_v \tag{6}$$

During the operation of OHP, the heat and mass transfer on the vapor-liquid interface is the root cause of the interface change [36]. To calculate the mass and heat transfer in the phase change process, Lee *et al.,* [34] proposed a mass transfer model, developed a complete set of CFD codes, and connected them to the control equation. After the mass transfer is determined, the heat transfer in the phase change process is calculated by the product of the mass transfer and the latent heat of vaporization, as shown in Eqs. (7)-(10) [37].

Evaporation ($T>T_{sat}$):

$$S_{m,l} = -\beta_l \alpha_l \rho_l \frac{T - T_{sat}}{T_{sat}} \tag{7}$$

$$S_{m,v} = \beta_l \alpha_l \rho_l \frac{T - T_{sat}}{T_{sat}} \tag{8}$$

Condensation ($T<T_{sat}$):

$$S_{m,l} = \beta_2 \alpha_v \rho_v \frac{T_{sat} - T}{T_{sat}} \tag{9}$$

$$S_{m,v} = -\beta_2 \alpha_v \rho_v \frac{T_{sat} - T}{T_{sat}} \tag{10}$$

2.2 Model Description

The OHP tube diameter must be small enough to allow the working fluid to form the vapor and liquid plugs distribution within the pipe. The critical diameter (D_{crit}) for the OHP must satisfy the conditions as described in Eq. (11) [38]. Through calculations, it is determined that the range of

diameters selected for the variable-diameter single-loop OHP in this study falls within the range of 2mm to 4mm.

$$0.7\sqrt{\frac{\sigma}{g(\rho_l-\rho_v)}} \leq D_{crit} \leq 1.8\sqrt{\frac{\sigma}{g(\rho_l-\rho_v)}} \tag{11}$$

The structure of the single-loop variable-diameter OHP is shown in Figure 1(a). It has a total length of 150 mm and is vertically oriented. From bottom to top, it consists of the evaporation section, the adiabatic section, and the condensation section, each with a length of 50 mm. The straight sections of the evaporator and condenser segments feature variable-diameter structures, with diameters D1 and D2 at the two ends and a diameter of D2 in the curved section. To reduce numerical dissipation, structured hexahedral grids were generated for the OHP flow field using ICEM. An O-block was created to address grid distortion at the vertices of curved blocks, and grid refinement was applied to the near-wall boundary layer grids. Figure 1(b) illustrates a schematic of the grid in a portion of the evaporation section, with grid refinement near the wall.

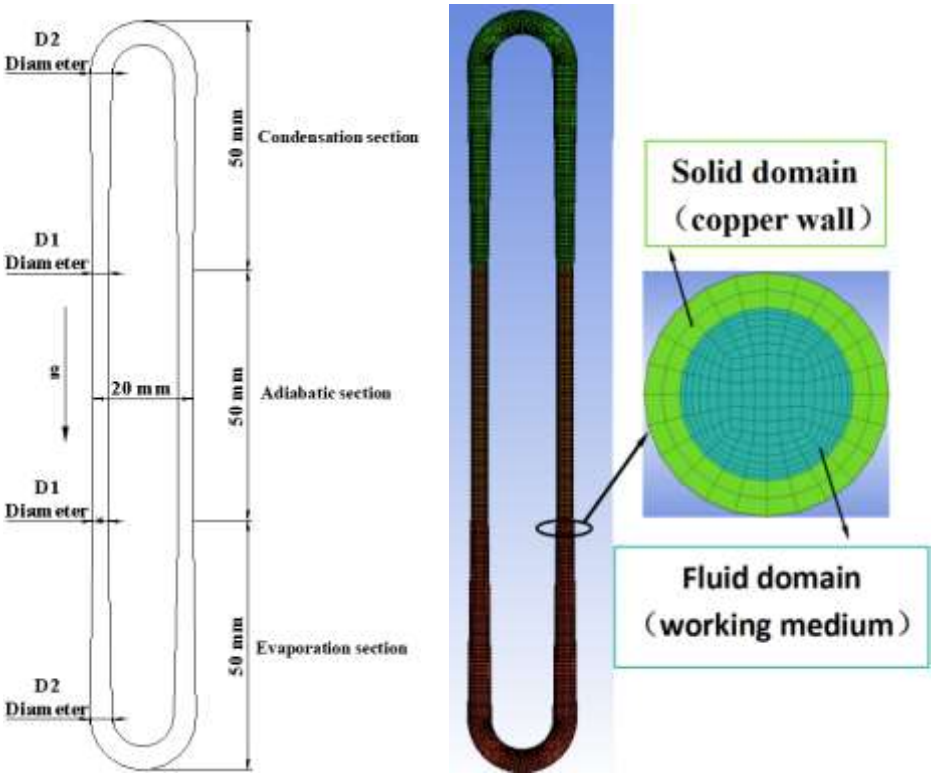

(a) (b)

Fig. 1. The variable diameters of the OHP model, (a) Structure diagram, (b) Grid structure diagram

Under the condition of keeping the volume of fluid domain in OHP unchanged, as shown in Table 1, four OHPs with different pipe diameter ratio k (D_2/D_1) are designed. When k=1, it is a common 3mm equal diameter OHP.

Table 1
OHPs with different pipe diameter ratios

Cases	Diameter ratio k	Diameter D1/mm	Diameter D2/mm	Fluid domain volume/mm^3
Case1	0.8	3.27mm	2.61mm	2215.3
Case2	1.0	3.00mm	3.00mm	2215.3
Case3	1.25	2.70mm	3.38mm	2215.4
Case4	1.5	2.44mm	3.66mm	2215.3

It is important to note that the tube wall is made of copper, and the working fluid is water, where the liquid phase is considered as the first phase and the vapor phase as the second phase. As shown in Table 2, REFPROP 9.0 software was used to obtain the thermophysical properties of water [33]. To facilitate the calculations and create a reasonably simplified mathematical model for the research, the following basic assumptions were made:

i) The initial temperatures of the vapor and liquid are both at saturation temperature.
ii) The liquid-vapor interface is at the saturation temperature.
iii) The vapor phase is treated as an ideal vapor.

Table 2
The thermophysical properties of water

Parameters	Formulas/values
ρ_l (kg/m^3)	$1002.7 - 0.1424T - 0.00326T^2 + 2.6544 \times 10^{-6} T^3$
ρ_v (kg/m^3)	Ideal Gas Law
$C_{p,l}$ (J/kg·K)	$4083.6 + 3.7701\,T - 0.0372\,T^2 + 1.4092 \times 10^{-4}T^3$
$C_{p,V}$ (J/kg·K)	$1563.1 + 1.6038\,T - 0.00293\,T^2 + 3.2161 \times 10^{-6}\,T^3$
λ_l (W/m·K)	$0.5656 + 0.00188\,T - 8.3481 \times 10^{-6}T^2 + 6.4842 \times 10^{-9}T^3$
λ_v (W/m·K)	0.0261
σ (N/m)	$0.09805856 - 1.845 \times 10^{-5}T - 2.3 \times 10^{-7}T^2$
μ_l (mPa·s)	$0.00133 - 2.1342 \times 10^{-5}T + 1.3826 \times 10^{-7}T^2 - 3.098 \times 10^{-10}T^3$
μ_v (mPa·s)	1.34×10^{-5}

The numerical simulation of the OHP can be divided into two stages, based on the actual physical processes. The first stage involves filling the working fluid into the OHP, where, under microscale influences, an initial distribution of vapor and liquid plugs forms. During this stage, all wall boundary conditions are set to the temperature of the condensation section (293.15K).

The second stage primarily simulates the startup and stable operation of the OHP under constant 40W heating conditions in the evaporation section. During this phase, the boundary conditions for the evaporator, adiabatic section, and condensation sections are as follows: constant heat flux, adiabatic, and constant temperature, respectively. The temperature in the condensation section is maintained at 293.15K, and the heat flux in the evaporation section is set as the ratio of the 40W heating power to the evaporation section's surface area.

In the simulation, all governing equations were solved using the Fluent Launcher 2021 R1 software based on the finite volume method. The primary mathematical models are presented in Table 3. Figure 2 is a flowchart of using Fluent to carry out simulation.

Table 3
Main mathematical models and parameters

Models	Parameters
Computational model	3D Transient
Solution algorithm	Segregated Implicit
Multiphase flow model	VOF Explicit
Phase setting	Primary-water and secondary-vapor
Gravity Item Settings	Y axis -9.81m/s^2
Surface tension model	CSF (0.0728N/m)
Viscous model	Realizable k-epsilon
pressure-velocity coupling method	PISO
Pressure discretization scheme	Body Force Weighted
Discrete scheme of momentum equation	2ed Order Upwind
Interface volume fraction interpolation algorithm	Geo-Reconstruct
Courant number	0.25
Fluid filling rates (FR)	50%

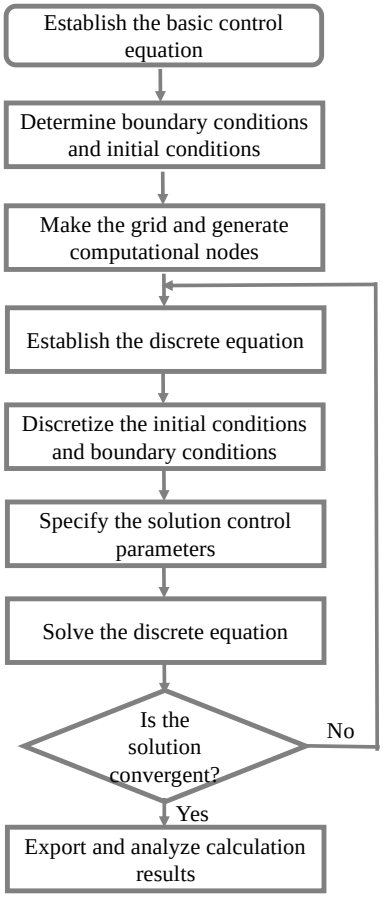

Fig. 2. CFD work flow chart

2.3 Validation of Model

To validate the grid independence and ensure the reliability of numerical results for Case 2 and other pipe diameter OHPs, four different grid sizes were employed. The corresponding thermal resistance was calculated for each grid size. As shown in Equation (12), thermal resistance R is employed to assess the heat transfer performance of the OHP. In the equation, T_{eva} and T_{con} denote

the average wall temperatures of the evaporator and condensation sections, respectively. Q represents the heating power applied to the evaporation section.

$$R = \frac{T_{eva} - T_{con}}{Q} \tag{12}$$

As shown in Figure 3. The number of grids is more than 200 thousand, and the deviation of the thermal resistance value obtained is not more than 1%, so the grid division scheme with the number of 231678 is adopted in this study.

To verify the effectiveness of the numerical model and keep the size parameters of the OHP consistent with those in the literature [39], the numerical calculation of the OHP in the literature was carried out, and the results are shown in Figure 4. The calculation results show that the trend of thermal resistance value obtained by numerical simulation is consistent with the experimental results, and the maximum relative error between the thermal resistance value and the literature value is 6.6%. In addition, by comparing the simulated flow pattern with the flow pattern obtained from the visualization experiment of Xu *et al.,* [40], it can also be found that the flow pattern of the numerical simulation better reflects the actual flow pattern of the experiment.

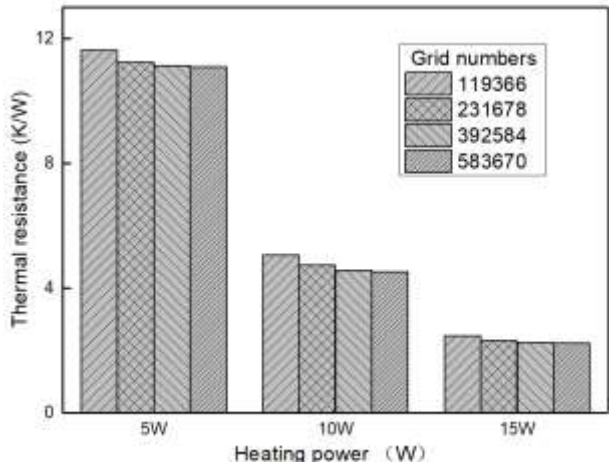

Fig. 3. Grid independence verification

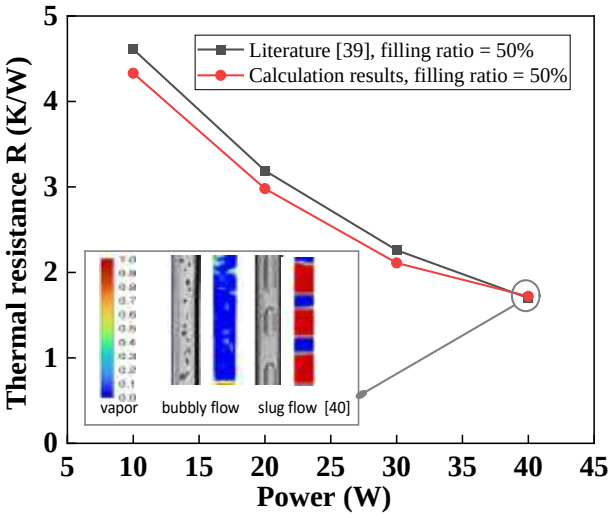

Fig. 4. Validation of present result with those of literature [39,40]

3.Results and Discussion

3.1 Initial Stage Analysis

After the working fluid is introduced into the OHP, under the influence of surface tension, gravity, and intermolecular forces between the wall, there is a tendency for the liquid phase to move towards the direction of minimizing its free energy [41]. Additionally, the attractive forces between the same phase working fluid molecules lead to gradual aggregation. Over time, as these trends accumulate, the OHP interior eventually forms a situation with alternating uniform distribution of vapor plugs and liquid slugs, resulting in a clearly defined interface between the vapor and liquid phases [42]. This initial phase of the working fluid's vapor-liquid distribution provides the foundation for the initiation of the OHP.

As shown from Figure 5(a), during the initial phase, the influence of gravity on the liquid phase is more pronounced. In different OHP configurations, the longest vapor plugs are all located at the top of the condensation section. The distribution of the longest liquid slugs is influenced by the pipe

diameter ratio and exhibits varying characteristics. In the case of a pipe diameter ratio (k) of 0.8, the longest liquid slugs are distributed in the adiabatic section. For configurations with an equal pipe diameter (k=1), the longest liquid slugs are near the top of the evaporation section. In comparison to equal diameter configurations, OHPs with pipe diameter ratios of k=1.25 and k=1.5 have longer liquid slugs distributed not only near the top of the evaporation section but also more dispersed within the evaporation section itself.

Figure 5(b) illustrates the distribution of vapor plugs for OHPs with different pipe diameter ratios. The number of liquid slugs in the condensation section is most affected by the varying pipe diameter. When compared to the k=1 configuration, in cases with pipe diameter ratios of k>1, the number of liquid slugs in the condensation section decreases from around 15 to 10. Among the four OHPs, the OHP with a pipe diameter ratio of k=0.8 has the fewest liquid slugs in the adiabatic section, totaling 15. Conversely, for the k=0.8 configuration, the evaporation section has the highest number of liquid slugs, reaching 21.

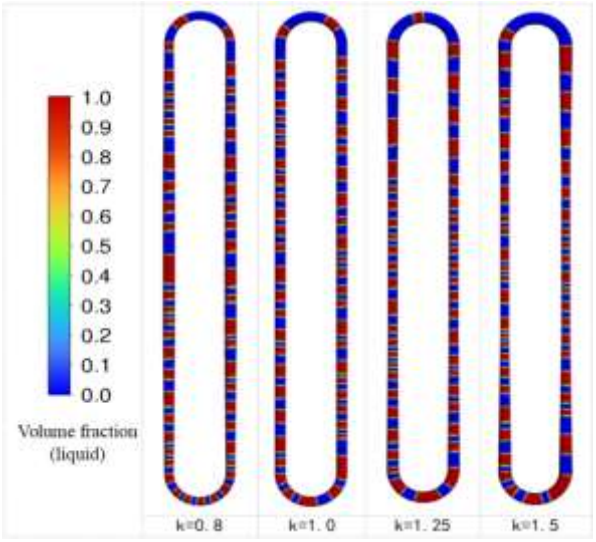

(a)

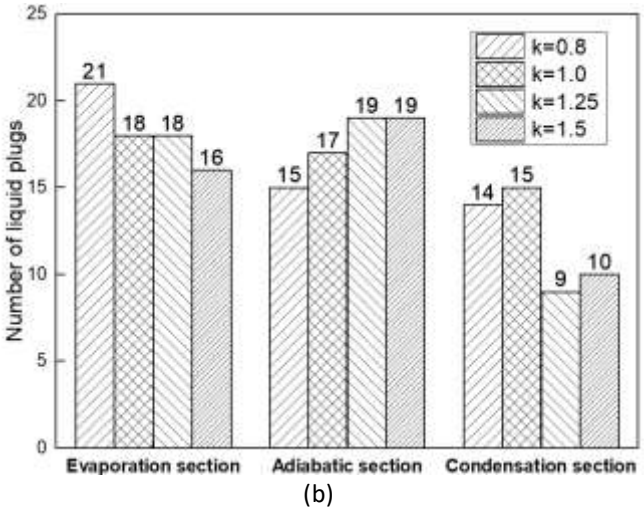

(b)

Fig. 5. Vapor and liquid plugs distribution characteristics in OHP with different pipe diameter ratios at the initial stage, (a) The liquid fraction variations, (b) Number of liquid slugs in different sections

3.2 Start-Up Stage Analysis

After the initial phase of calculations, the OHP contains a random distribution of vapor plugs and liquid slugs. The OHP enters the startup phase when a constant heat flux boundary condition is applied to the evaporation section. During the startup phase, the working fluid inside different OHPs undergoes three distinct processes: simultaneous upward flow in the channels, unidirectional cyclic flow, and reverse flow [43]. Taking a straight-tube OHP with a diameter ratio of 1 (k=1) as an example, the characteristics of vapor-phase distribution, temperature field, and pressure field during the startup phase are explored, as shown in Figure 6-8.

As the walls of the evaporation section are heated, nucleate boiling occurs within the fluid, leading to the random formation of vapor cores that generate small vapor bubbles. Simultaneously, the existing vapor plugs initially located in the evaporation section expand as the liquid film evaporates. Since the heating surfaces of the OHP's evaporation section are symmetrically arranged, as depicted in Figure 6, the distribution of vapor and liquid can be observed. During the first 1 to 2 seconds of heating, the vapor plugs in both channels of the evaporation section move towards the condensation section due to the expansion effect. At the same time, in the condensation section, the pressure inside the OHP increases, resulting in a higher saturation temperature. Since the temperature of the vapor plugs in the evaporation section is lower than this new saturation temperature, the vapor plugs start to condense and shrink until they transform into smaller vapor bubbles. This condensation process causes two adjacent liquid slugs to come into contact, forming a larger liquid slug. After 2.5 seconds, the fluid inside the tube begins to flow in the clockwise direction and exhibits accelerated movement. This is primarily due to the increasing pressure difference between the left and right channels of the OHP's evaporation section as the vapor-liquid film within the evaporation section continues to evaporate. When the pressure difference becomes sufficient to overcome gravity and shear forces, the fluid inside the tube starts to flow in the same direction, and the gravitational force that initially hindered the flow of liquid working fluid from the condensation section to the evaporation section transforms into a driving force. However, after 3.5 seconds, almost all the liquid working fluid flows from the condensation section to the evaporation section, and the gravitational force acting on the liquid working fluid becomes a resistance. By the 4-second mark, the working fluid not only fails to flow in the clockwise direction but exhibits slow counterclockwise oscillations. This is because the substantial influx of low-temperature liquid working fluid into the condensation section cools down the evaporation section, making it difficult for the evaporator and condensation sections to establish a sufficient pressure difference to drive the working fluid to continue flowing clockwise.

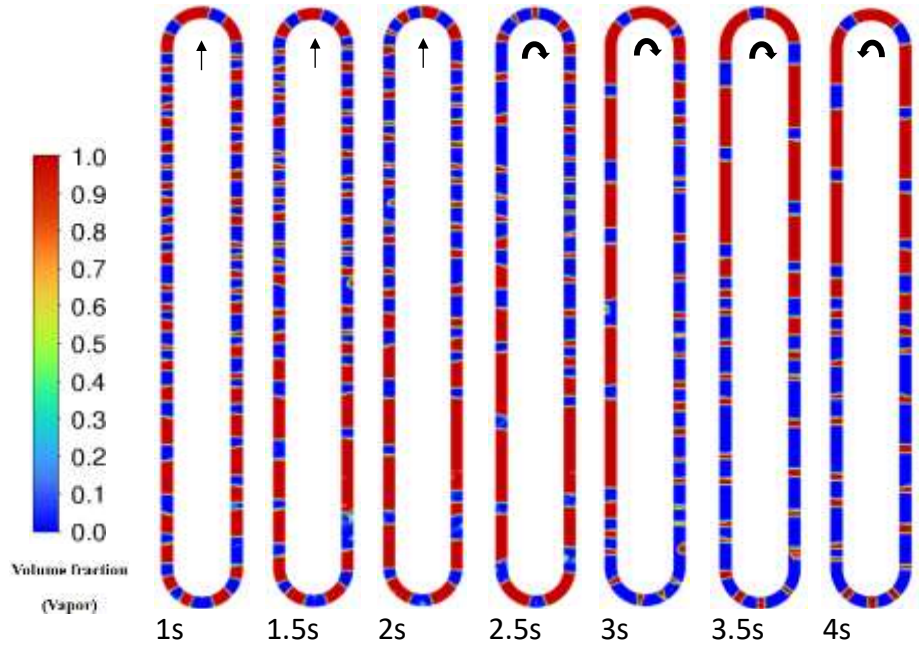

Fig. 6. Vapor phase distribution of transient cloud field in the OHP at start-up stage (k=1.0)

In Figure 7, the temperature distribution within the tube at different times is depicted. During the 1 to 2-second interval, the fluid in the evaporation section is heated by the tube wall, causing its temperature to rise continuously. Notably, the vapor plugs experience a rapid temperature increase, quickly reaching the wall temperature. In contrast, the temperature increase in the liquid slugs is slower, primarily due to the substantial latent heat required for the liquid working fluid to evaporate into a vapor [44]. As the vapor plugs expand along the two channels in the evaporation section after 2.5 seconds, the temperature rises within the adiabatic section near the evaporation section. The fluid inside the tube exhibits a significant temperature gradient along the direction of fluid flow in the evaporation section. After 2.5 seconds, as the working fluid flows clockwise, the low-temperature working fluid from the condensation section flows downward into the evaporation section from the right, while the high-temperature working fluid from the left flows upward into the condensation section. This leads to a noticeable temperature difference within the tube. The high temperature working fluid within the evaporation section cools rapidly upon reaching the condensation section, and the vapor plug's temperature drops very quickly, reaching around 293.15K, which is the wall temperature. The entry of the low temperature working fluid, especially the liquid phase, into the evaporation section significantly reduces the maximum and average temperatures within the evaporation section. By the 3.5-second mark, the highest temperature drops from 333.6K at 3 seconds to 325.3K. After 4 seconds, due to the low-speed oscillatory motion of the fluid inside the tube, the working fluid in the evaporation section absorbs heat from the tube wall, causing it to rise in temperature to the saturation temperature, leading to the onset of nucleate boiling. Meanwhile, the working fluid in the condensation section continues to cool. As the temperature difference between the evaporator and condensation sections increases, the OHP prepares for the next cycle of fluid circulation.

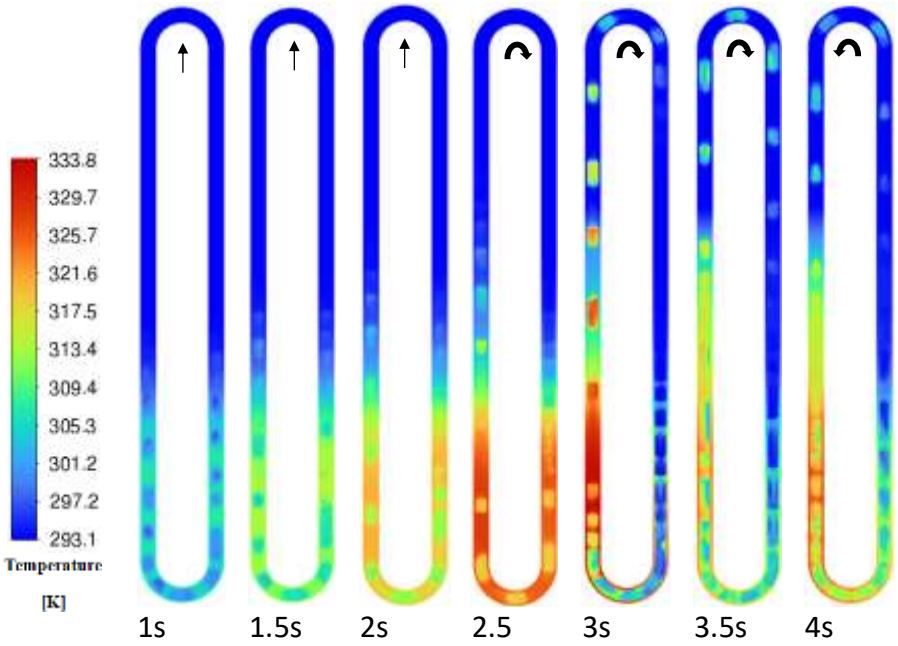

Fig. 7. Temperature distribution of transient cloud field in the OHP at start-up stage (k=1.0)

Figure 8 illustrates the pressure distribution within the pipe at different time points. Overall, the internal pressure in the OHP exhibits a gradient, influenced by gravity, with the high-pressure region consistently located in the evaporation section, and the highest pressure occurring at the bottom of the evaporator [45]. During the period from 1 to 2 seconds, as the working fluid in the evaporation section is heated and undergoes an increase in temperature, the overall pressure within the pipe rises, and the pressure distribution in the channels on both sides of the adiabatic section becomes more disparate. By 2.5 seconds, the pressure difference between the channels on both sides is sufficient to overcome gravity and shear forces, enabling unidirectional flow of the working fluid. At 3 seconds, a large amount of low-temperature liquid-phase working fluid rapidly flows into the lower part of the evaporation section, resulting in a "J"-shaped pressure differential distribution in the evaporation section. By 4 seconds, as the working fluid within the pipe undergoes oscillatory and slow counterclockwise movement, the pressure distribution in the channels on both sides of the evaporation section returns to a state with minimal differences.

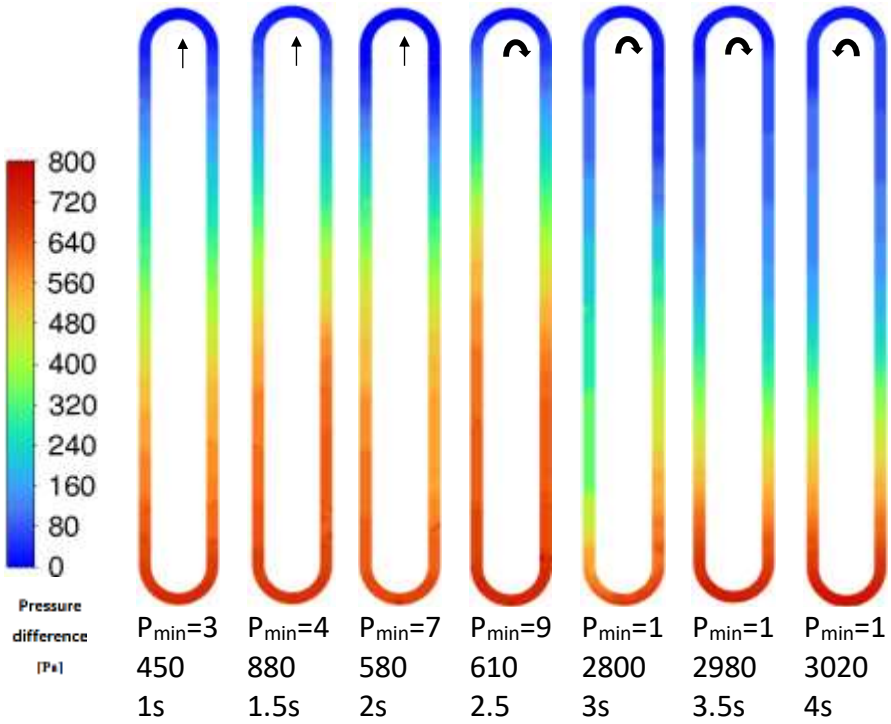

Fig. 8. Pressure difference distribution of transient cloud field in the OHP at start-up stage (k=1.0)

The variation in working fluid temperature serves as a crucial indicator for assessing the successful initiation of the OHP. Figure 9 depicts the transient time corresponding to the first occurrence of temperature peaks and troughs in the evaporation section during the startup phase. It is evident from Figure 9 that the OHP with a diameter ratio of 0.8 reaches its first temperature peak at approximately 2.24 seconds, approximately 0.6 seconds earlier than the other OHPs. This is primarily due to the larger diameter in the adiabatic section, where there is initially a greater amount of liquid-phase working fluid. In contrast, the smaller diameter in the evaporation section makes it easier for vaporized cores to generate vapor plugs in the confined space, resulting in the working fluid in the OHP with a diameter ratio of 0.8 transitioning from upward flow to unidirectional flow earlier. The three OHPs with diameter ratios of 1.0, 1.25, and 1.5 exhibit minor differences in the moment of first temperature peaks, occurring at 2.82 seconds, 2.86 seconds, and 2.8 seconds, respectively. However, there are significant differences in temperatures, measuring 328.1K, 325.0K, and 324.2K, respectively. This is primarily due to the increased diameter ratio, leading to a larger spatial flow domain in the evaporation section. Consequently, the larger amount of working fluid being heated results in a slower temperature increase. As the working fluid within the pipe transitions from upward flow to unidirectional flow, a substantial amount of low-temperature liquid enters the evaporation section, causing a rapid decrease in surface temperature. The temperature trough values in the evaporation section for OHPs with different diameter ratios are 313.0K, 317.4K, 315.0K, and 314.7K, with time lags relative to the temperature peaks of 0.58 seconds, 0.58 seconds, 0.82 seconds, and 0.81 seconds, respectively.

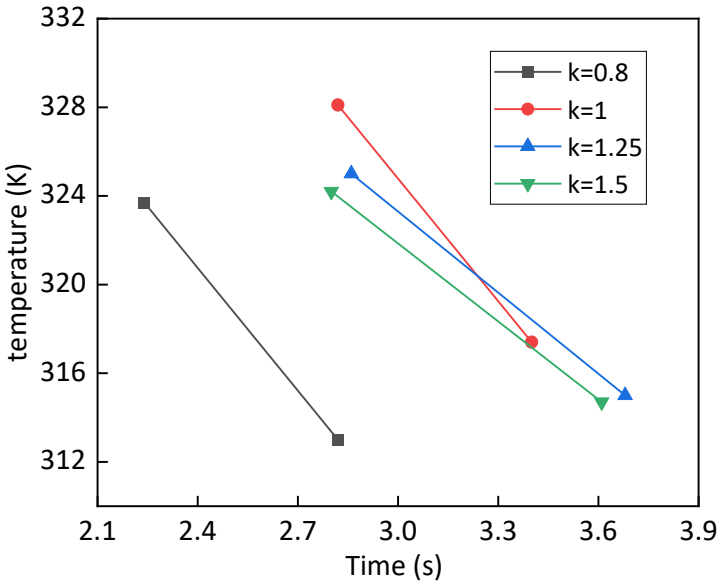

Fig. 9. The evaporator temperature and time of the first start-up with different pipe diameter ratios

Figure 10 illustrates the dynamic changes in vapor phase distribution for OHPs with different diameter ratios during the startup phase between 6 and 14 seconds. To ensure that small vapor plugs are not reduced or disappeared due to condensation, the longest vapor plug at the 6th-second transient is tracked and denoted as 1#-vapor plug. It is evident from the composite figures that in the vicinity of the evaporation section near the adiabatic section, there is a substantial mixture of vapor and liquid in proximity to the wall, indicating that the liquid phase is heated to generate bubbles, which serve as the driving pressure for the circulation of the working fluid within the tube. It's worth noting that in the OHP with a diameter ratio of 0.8, bubbles are formed on the right straight tube wall, whereas in the other diameter ratios, bubbles form on the left straight tube wall. This discrepancy arises from the fact that the working fluid inside the OHP with a diameter ratio of 0.8 flows clockwise, while in the other diameter ratios, the working fluid in the OHP flows counterclockwise [46].

The greater the velocity within a unit of time, the greater the displacement. In the OHP with a diameter ratio of 1, the 1#-vapor plug covers a distance exceeding one full revolution during the tracked time frame. However, in the other diameter ratios, the displacement of the 1#-vapor plug remains less than one full revolution. The 1#-vapor plug in the OHP with diameter ratios of 1.25 and 1.5 has displacements close to one full revolution but does not complete it. Notably, in the OHP with a diameter ratio of 0.8, the 1#-vapor plug exhibits the shortest displacement, covering only 3/4 of a full revolution. This indicates that when the diameter ratio is 1, the average flow velocity of the working fluid inside the tube is the highest, whereas for diameter ratios smaller than 1, the flow velocity of the working fluid within the tube is the lowest.

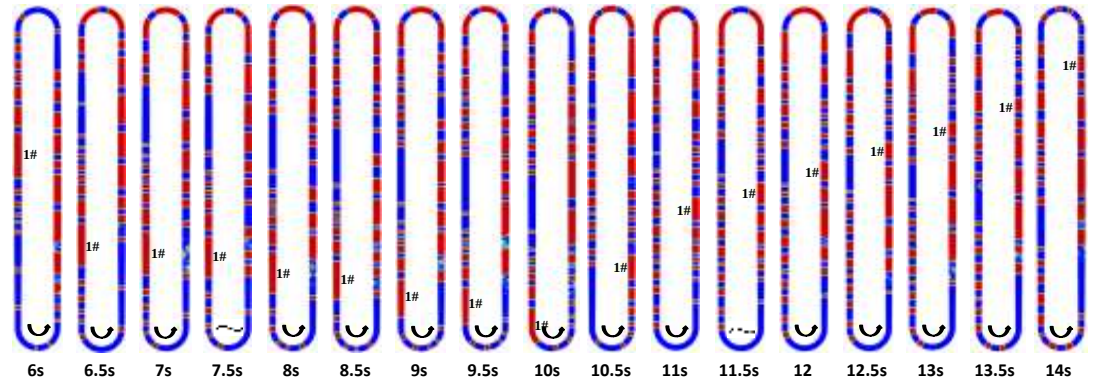

(a)

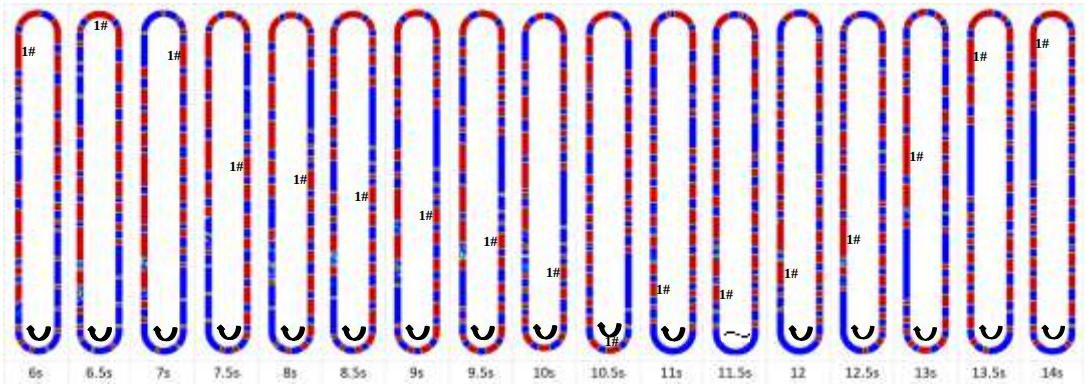

(b)

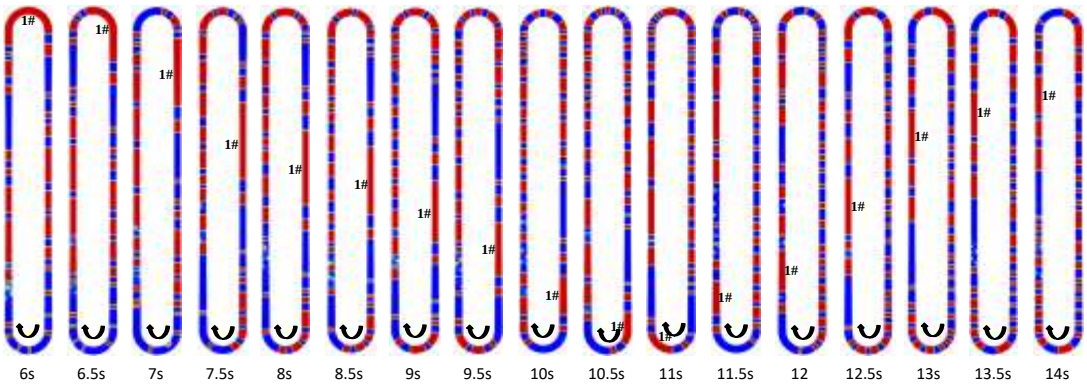

(c)

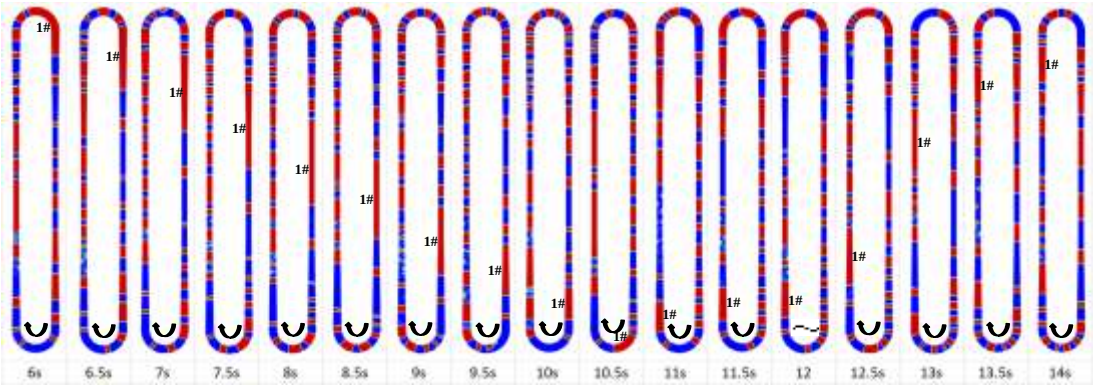

(d)

Fig. 10. Vapor phase distribution of transient cloud field in the OHP with different pipe diameter ratios, (a) k=0.8, (b) k=1.0, (c) k=1.25, (d) k=1.50

3.3 Stable Operations Stage Analysis

The temperature change is an important indicator to judge whether OHP is successfully started [47]. Figure 11 (a) shows the average temperature T_{eva} change curve of copper wall surface in the evaporation section of OHP. It can be seen from the figure that, as the OHP enters the startup phase, the wall temperature of the evaporation section of OHP with different pipe diameter ratios rises in oscillation. With the passage of time, as the working fluids in different OHPs successively form stable circulating flow, the wall temperature oscillation also begins to stabilize. The pipe diameter ratio has a great influence on the temperature oscillation of OHPs. The peak value of the temperature oscillation of the OHP with a pipe diameter ratio of 0.8 is much higher than that of other OHPs, up to 402.3K, and the temperature oscillation does not converge in the calculated period, indicating that the OHP with a pipe diameter ratio of 0.8 has experienced heat transfer deterioration under the heating power of 40W. The peak temperature of the equal diameter OHP (k=1) is 381.4K, and the corresponding time is 26.9s. The peak values of temperature oscillation of OHPs with pipe diameter ratio of 1.25 and 1.5 are both small and basically the same, which are 357.9K and 358.6K respectively. It is worth noting that after the OHP is heated to 20s, the temperature oscillations of the OHPs with pipe diameter ratios of 1, 1.25 and 1.5 converge gradually. The temperature oscillations of OHP with pipe diameter ratio of 1 are larger, ranging from 351.1K to 374.6K, with a difference of 23.5K. The temperature oscillations of the OHPs with pipe diameter ratios of 1.25 and 1.5 are 348.3K to 357.7K, 350.4K to 358.3K, with a difference of 9.4K and 7.9K. In short, the temperature oscillation amplitude decreases gradually with the increase of pipe diameter ratio. Taking the 15s to 35s period as the statistical interval, the oscillation frequencies of OHPs with pipe diameter ratios of 0.8, 1.0, 1.25 and 1.5 are obviously different, which has been oscillated for 3, 4, 8 and 7 times respectively.

The OHP structure with large pipe diameter ratio is conducive to improving the temperature oscillation frequency. Figure 11 (b) shows the thermal resistance of the OHPs with different pipe diameter ratios. Corresponding to the temperature curve, the thermal resistance of OHPs with pipe diameter ratios of 1.25 and 1.5 is smaller than that of OHP with equal pipe diameter (k=1), Which the values are 1.50K/W and 1.53K/W respectively. However, the heat transfer performance of the OHP with the pipe diameter ratio of 0.8 decreased significantly, and the thermal resistance was 2.22K/W, which was 27.6% higher than that of the OHP with the pipe diameter ratio of 1.

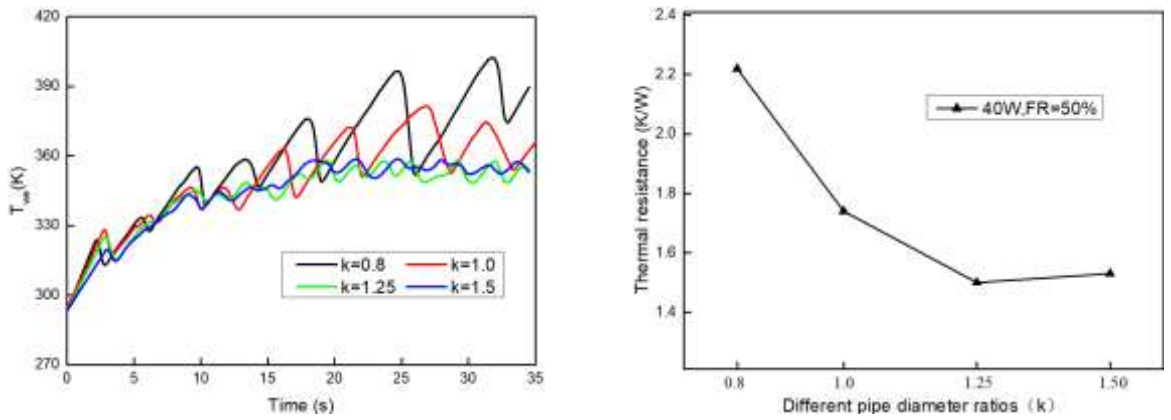

(a) (b)

Fig. 11. Temperature curves and thermal resistance of OHP with different pipe diameter ratios, (a) Temperature curves, (b) Thermal resistance of the OHPs

The heat of the working medium in the OHP is taken away by the wall of the condensation section. Figure 12 shows the instantaneous cooling power curve of the wall of the condensation section. The

cooling power oscillation curves of OHPs with different pipe diameter ratios are very different. According to the temperature curve in Figure 8, the peak value of cooling power oscillation increases with the increase of temperature in the tube. The OHP with a pipe diameter ratio of 0.8 has the worst heat dissipation, and there are only four strong oscillations with a cooling power greater than 40W. The cooling power of the equal diameter OHP (k=1) is greater than 40W for 6 times, and reaches 101.6W at 21.8s. Compared with pulse OHPs with tube diameter ratios of 0.8 and 1.0, the number of thermal transient power oscillations of 1.25 and 1.5 type OHPs with tube diameter ratios greater than 40W is significantly increased, and the period of cooling power greater than 40W in the oscillation cycle is longer, including 14 for 1.25 type OHPs, which is conducive to further reducing the temperature in the pipe. Compared with pipe diameter ratios of 0.8 and 1.0, the number of power oscillations greater than 40W is significantly increased for OHPs with pipe diameter ratios of 1.25 and 1.5, and the period when the cooling power is greater than 40W is longer. The OHP with pipe diameter ratios of 1.25 has 14 times oscillations, which is conducive to further reducing the temperature in the pipe. In the early period of time, the oscillation pattern of the OHP with the pipe diameter ratio of 1.5 is like that of the OHP with the pipe diameter ratio of 1.25. However, the cooling power oscillation frequency of the OHP with the pipe diameter ratio of 1.5 is significantly accelerated after the 25s, and the peak cooling power is smaller than that of the OHP with the pipe diameter ratio of 1.25 at the same period. This high-frequency and low amplitude cooling power oscillation is conducive to reducing the temperature oscillation range of the OHP.

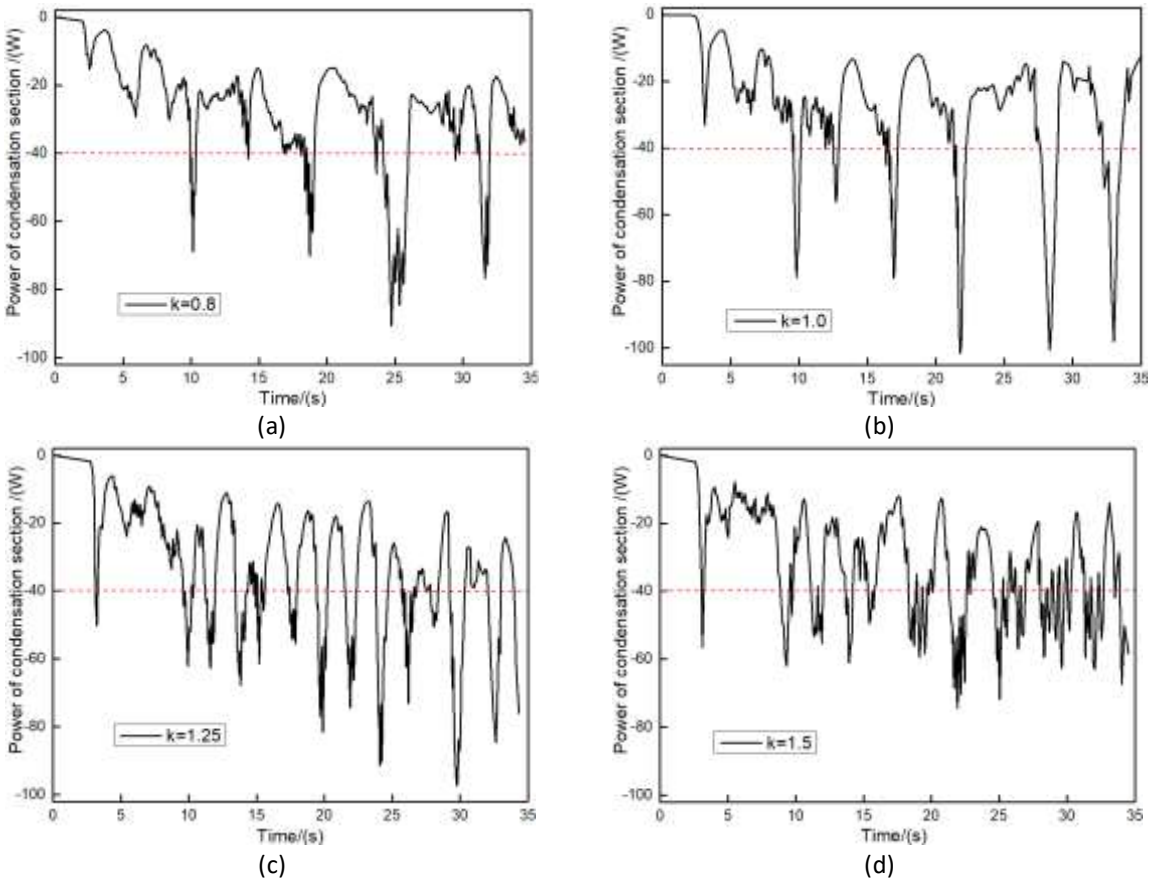

Fig. 12. Instantaneous cooling power curves of condensation section wall, (a) k=0.8, (b) k=1.0, (c) k=1.25, (d) k=1.5

The research object is the straight part on the side where the working medium flows out of the evaporation section in the OHP. Figure 13 shows the distribution of velocity cloud field when the OHP

with different pipe diameter ratios are heated to about 10s and the cooling power of the condensing section has a peak. The corresponding sampling time of case 1-4 OHPs is 10.15s, 9.84s, 9.94s, 9.33s, and the corresponding peak heat release power is 48.6W, 78.8W, 62.1W, 62W, respectively. The working fluid movement in the OHP has a great influence on the performance of heat transfer. From the velocity cloud field diagram, the working medium flow velocity at both ends of the evaporation section and insulation section of the OHP with a pipe diameter ratio of 0.8 is relatively large, and the top of the evaporation section can reach 0.29m/s. However, the gradient of the velocity field in the evaporation section is uniform, the wall velocity is small, and the middle velocity is large, which indicates that there is less turbulence in the regional field, which is not conducive to the mutual transformation of vapor and liquid phases and heat transfer. The OHP with a pipe diameter ratio of 0.8 has the largest diameter in the insulation section, where there is a large area of turbulence, indicating that there is a strong vapor and liquid phases mutation [48].The fluid velocity field in OHP with equal diameter (k=1) is relatively uniform, and the turbulent flow is more obvious in the area where the evaporation section and the insulation section are connected, because the liquid phase is heated and boiling in the area. As the OHP with pipe diameter ratio of 1.25 and 1.5 are small in the insulation section, the flow velocity of working medium in the insulation section is relatively large. As the pipe diameter ratio of 1.5 type OHP is larger and the pipe diameter in the insulation section is smaller, the flow velocity in the insulation section is the highest, and the peak flow velocity in the center of working medium is 0.41m/s. Compared with other OHPs, the flow velocity of the OHPs with a pipe diameter ratio of 1.25 and 1.5 in the evaporation section and the condensation section is smaller, and the turbulent flow area of the fluid in the evaporation section is large, which is conducive to the full heat transfer of the fluid in this area, and promotes the cooling of liquid medium and the condensation of the vapor.

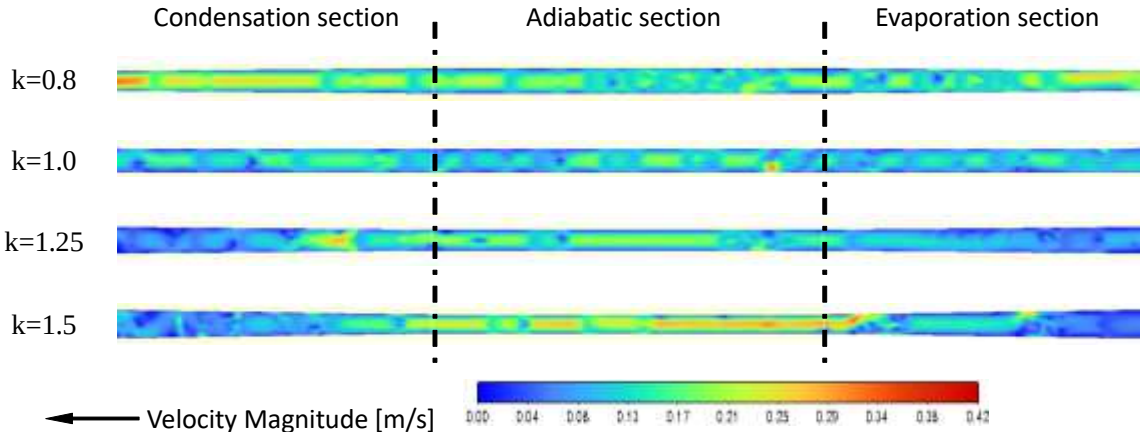

Fig. 13. Velocity flow field diagram of the OHPs with different pipe diameter ratios

4. Conclusions

This study establishes a mathematical model using the VOF two-phase flow approach to analyze single-loop OHPs with varying diameter ratios. Key findings include:

i) In the initial phase of OHP operation, the number of liquid slugs in the condensation section is highly sensitive to the diameter ratio, with 9–10 slugs at diameter ratios of 1.25 and 1.5, compared to 15 slugs at a ratio of 1.

ii) OHPs with a diameter ratio of 0.8 show the fastest startup but suffer from a 27.6% increase in thermal resistance at 40W. Optimal heat transfer performance occurs at a diameter ratio of 1.25, surpassing that of uniform diameter OHPs.
iii) Larger diameter ratios decrease fluid velocity across the OHP but enhance turbulence, improving heat exchange efficiency.
iv) Increasing the diameter ratio leads to more frequent but lower-amplitude temperature oscillations, contributing to greater operational stability.

Acknowledgement
This research was funded by the Science and Technology Research Project of Jiangxi Provincial Department of Education (GJJ2404911), the Ministry of Higher Education, Malaysia through the Fundamental Research Grant Scheme: FRGS/1/2024/TK10/UMP/02/15 and Universiti Malaysia Pahang Al-Sultan Abdullah (RDU240117).

References

[1] Shetty, Divya D., Mohammad Zuber, K. N. Chethan, G. Laxmikant, Irfan Anjum Badruddin Magami, and Chandrakant R. Kini. "Advancements in Battery Thermal Management for High-Energy-Density Lithium-Ion Batteries in Electric Vehicles: A Comprehensive Review." *CFD Letters* 16, no. 9 (2024): 14-38. https://doi.org/10.37934/cfdl.16.9.1438
[2] Li, Ziyong, Hailiang Luo, Yuguang Jiang, Haichao Liu, Lian Xu, Kunyuan Cao, Hongjie Wu, Peng Gao, and Hong Liu. "Comprehensive review and future prospects on chip-scale thermal management: Core of data center's thermal management." *Applied Thermal Engineering* (2024): 123612. https://doi.org/10.1016/j.applthermaleng.2024.123612
[3] Rahman, SM Imrat, Ali Moghassemi, Ali Arsalan, Laxman Timilsina, Phani Kumar Chamarthi, Behnaz Papari, Gokhan Ozkan, and Christopher S. Edrington. "Emerging trends and challenges in thermal management of power electronic converters: A state of the art review." *IEEE Access* (2024). https://doi.org/10.1109/ACCESS.2024.3385429
[4] Basri, Mahamad Hisyam Mahamad, Zulkhairi Kamaruzaman, Fairosidi Idrus, Norasikin Hussin, and Idris Saad. "Heat Pipe as a Passive Cooling Device for PV Panel Performance Enhancement." *Journal of Advanced Research in Applied Sciences and Engineering Technology* 28, no. 2 (2022): 190-198. https://doi.org/10.37934/araset.28.2.190198
[5] Akachi, Hisateru. "Structure of heat pipe." *United States patent, Patent No. 4921041* (1990).
[6] Ayel, Vincent, Maksym Slobodeniuk, Rémi Bertossi, Cyril Romestant, and Yves Bertin. "Flat plate pulsating heat pipes: A review on the thermohydraulic principles, thermal performances and open issues." *Applied Thermal Engineering* 197 (2021): 117200. https://doi.org/10.1016/j.applthermaleng.2021.117200
[7] Kim, Wookyoung, and Sung Jin Kim. "Fundamental issues and technical problems about pulsating heat pipes." *Journal of Heat Transfer* 143, no. 10 (2021): 100803. https://doi.org/10.1115/1.4050077
[8] Dave, Chirag, Prajwal Dandale, Kushagra Shrivastava, Dashrath Dhaygude, Kavi Rahangdale, and Nilesh More. "A review on pulsating heat pipes: latest research, applications and future scope." *Journal of Thermal Engineering* 7, no. 3 (2021): 387-408. https://doi.org/10.18186/thermal.878983
[9] Cataldo, Filippo, Jackson B. Marcinichen, and John R. Thome. "Mini-scale pulsating heat pipe cooling systems for high-heat-flux electronic equipment." In *Journal of Physics: Conference Series*, vol. 1868, no. 1, p. 012009. IOP Publishing, 2021. https://doi.org/10.1088/1742-6596/1868/1/012009
[10] Li, Zhi, and Li Jia. "Experimental study on natural convection cooling of LED using a flat-plate pulsating heat pipe." *Heat Transfer Research* 44, no. 1 (2013). https://doi.org/10.1615/HeatTransRes.2013006479
[11] Kavoosi Balotaki, Hassan, and Mohammad Hassan Saidi. "Design and performance of a novel hybrid photovoltaic–thermal collector with pulsating heat pipe (PVTPHP)." *Iranian Journal of Science and Technology, Transactions of Mechanical Engineering* 43 (2019): 371-381. https://doi.org/10.1007/s40997-018-0164-y
[12] Xu, Yanyan, Yanqin Xue, Weihua Cai, Hong Qi, and Qian Li. "Experimental study on performances of flat-plate pulsating heat pipes without and with thermoelectric generators for low-grade waste heat recovery." *Applied Thermal Engineering* 225 (2023): 120156. https://doi.org/10.1016/j.applthermaleng.2023.120156
[13] Mahajan, Govinda, Heejin Cho, Scott M. Thompson, Harrison Rupp, and Kevin Muse. "Oscillating heat pipes for waste heat recovery in HVAC systems." In *ASME International Mechanical Engineering Congress and Exposition*, vol. 57502, p. V08BT10A003. American Society of Mechanical Engineers, 2015. https://doi.org/10.1115/IMECE2015-52720

[14] Wu, Ze, Youqiang Xing, Lei Liu, Peng Huang, and Guolong Zhao. "Design, fabrication and performance evaluation of pulsating heat pipe assisted tool holder." *Journal of Manufacturing Processes* 50 (2020): 224-233. https://doi.org/10.1016/j.jmapro.2019.12.054

[15] Zhu, Liang, Linpei Zhu, and Shuangfeng Wang. "Experimental investigation on rotational oscillating heat pipe for in-wheel motor cooling of urban electric vehicle." *International Communications in Heat and Mass Transfer* 151 (2024): 107209. https://doi.org/10.1016/j.icheatmasstransfer.2023.107209

[16] Hongkun, Lu, M. M. Noor, Yu Wenlin, K. Kadirgama, I. A. Badruddin, and S. Kamangar. "Experimental research on heat transfer characteristics of a battery liquid-cooling system with⊥-shaped oscillating heat pipe under pulsating flow." *International Journal of Heat and Mass Transfer* 224 (2024): 125363. https://doi.org/10.1016/j.ijheatmasstransfer.2024.125363

[17] Shetty, Divya D., Mohammad Zuber, K. N. Chethan, G. Laxmikant, Irfan Anjum Badruddin Magami, and Chandrakant R. Kini. "Advancements in Battery Thermal Management for High-Energy-Density Lithium-Ion Batteries in Electric Vehicles: A Comprehensive Review." *CFD Letters* 16, no. 9 (2024): 14-38. https://doi.org/10.37934/cfdl.16.9.1438

[18] Bastakoti, Durga, Hongna Zhang, Da Li, Weihua Cai, and Fengchen Li. "An overview on the developing trend of pulsating heat pipe and its performance." *Applied Thermal Engineering* 141 (2018): 305-332. https://doi.org/10.1016/j.applthermaleng.2018.05.121

[19] Nazari, Mohammad Alhuyi, Mohammad H. Ahmadi, Roghayeh Ghasempour, Mohammad Behshad Shafii, Omid Mahian, Soteris Kalogirou, and Somchai Wongwises. "A review on pulsating heat pipes: from solar to cryogenic applications." *Applied energy* 222 (2018): 475-484. https://doi.org/10.1016/j.apenergy.2018.04.020

[20] Pagliarini, Luca, Naoko Iwata, and Fabio Bozzoli. "Pulsating heat pipes: Critical review on different experimental techniques." *Experimental Thermal and Fluid Science* 148 (2023): 110980. https://doi.org/10.1016/j.expthermflusci.2023.110980

[21] Khandekar, Sameer, Pradipta K. Panigrahi, Frédéric Lefèvre, and Jocelyn Bonjour. "Local hydrodynamics of flow in a pulsating heat pipe: a review." *Frontiers in Heat Pipes* 1, no. 2 (2010): 023003. https://doi.org/10.5098/fhp.v1.2.3003

[22] Noh, Hyung Yun, and Sung Jin Kim. "Numerical simulation of pulsating heat pipes: Parametric investigation and thermal optimization." *Energy conversion and management* 203 (2020): 112237. https://doi.org/10.1016/j.enconman.2019.112237

[23] Lee, Jungseok, and Sung Jin Kim. "Effect of channel geometry on the operating limit of micro pulsating heat pipes." *International Journal of Heat and Mass Transfer* 107 (2017): 204-212. https://doi.org/10.1016/j.ijheatmasstransfer.2016.11.063

[24] Pietrasanta, Luca, Daniele Mangini, Davide Fioriti, Nicolas Miche, Manolia Andredaki, Anastasios Georgoulas, Lucio Araneo, and Marco Marengo. "A single Loop pulsating heat pipe in varying gravity conditions: experimental results and numerical simulations." In *The 16th International Heat Transfer Conference: IHTC-16*, pp. 4877-4884. Begell House, 2018. https://doi.org/10.1615/IHTC16.her.023891

[25] Opalski, Marcin, Cezary Czajkowski, Przemysław Błasiak, Andrzej Ireneusz Nowak, Jun Ishimoto, and Sławomir Pietrowicz. "Comprehensive numerical modeling analysis and experimental validation of a multi-turn pulsating heat pipe." *International Communications in Heat and Mass Transfer* 159 (2024): 107990. https://doi.org/10.1016/j.icheatmasstransfer.2024.107990

[26] Mushan, Sagar G., and Vaibhav N. Deshmukh. "A review of pulsating heat pipes encompassing their dominant factors, flexible structure, and potential applications." *International Journal of Green Energy* (2024): 1-38. https://doi.org/10.1080/15435075.2024.2319229

[27] Xie, Fubo, Xinlong Li, Peng Qian, Zizhen Huang, and Minghou Liu. "Effects of geometry and multisource heat input on flow and heat transfer in single closed-loop pulsating heat pipe." *Applied Thermal Engineering* 168 (2020): 114856. https://doi.org/10.1016/j.applthermaleng.2019.114856

[28] Wang, Jiansheng, Yu Pan, and Xueling Liu. "Investigation on start-up and thermal performance of the single-loop pulsating heat pipe with variable diameter." *International Journal of Heat and Mass Transfer* 180 (2021): 121811. https://doi.org/10.1016/j.ijheatmasstransfer.2021.121811

[29] Kang, Zhanxiao, Dahua Shou, and Jintu Fan. "Numerical study of a novel Single-loop pulsating heat pipe with separating walls within the flow channel." *Applied Thermal Engineering* 196 (2021): 117246. https://doi.org/10.1016/j.applthermaleng.2021.117246

[30] Kang, Zhanxiao, Dahua Shou, and Jintu Fan. "Numerical study of single-loop pulsating heat pipe with porous wicking layer." *International Journal of Thermal Sciences* 179 (2022): 107614. https://doi.org/10.1016/j.ijthermalsci.2022.107614

[31] Fallahzadeh, Rasoul, Latif Aref, Fabio Bozzoli, Luca Cattani, and Hormoz Gholami. "A novel triple-diameter pulsating heat pipe: Flow regimes and heat transfer performance." *Thermal Science and Engineering Progress* 42 (2023): 101902. https://doi.org/10.1016/j.tsep.2023.101902

[32] Cheng, Po-Shen, and Shwin-Chung Wong. "Detailed visualization experiments on the start-up process and stable operation of pulsating heat pipes: Effects of internal diameter." *International Journal of Heat and Fluid Flow* 106 (2024): 109325. https://doi.org/10.1016/j.ijheatfluidflow.2024.109325
[33] Liu, Yuewen, Dan Dan, Mingshan Wei, Siyu Zheng, and Jixian Sun. "Numerical investigation on the start-up and heat transfer performance of dual-diameter pulsating heat pipes." *Applied Thermal Engineering* 236 (2024): 121709. https://doi.org/10.1016/j.applthermaleng.2024.121709
[34] Lee, W. H., and R. W. Lyczkowski. "The basic character of five two-phase flow model equation sets." *International journal for numerical methods in fluids* 33, no. 8 (2000): 1075-1098. https://doi.org/10.1002/1097-0363(20000830)33:8<1075::AID-FLD43>3.0.CO;2-5
[35] Hirt, Cyril W., and Billy D. Nichols. "Volume of fluid (VOF) method for the dynamics of free boundaries." *Journal of computational physics* 39, no. 1 (1981): 201-225. https://doi.org/10.1016/0021-9991(81)90145-5
[36] Choi, Benjamin Y., and Markus Bussmann. "A piecewise linear approach to volume tracking a triple point." *International journal for numerical methods in fluids* 53, no. 6 (2007): 1005-1018. https://doi.org/10.1002/fld.1317
[37] Shi, Xiaojun, Bangtao Yin, Gangqing Chen, Xiaodong Zhang, and Xuesong Mei. "Numerical study on two-phase flow and heat transfer characteristics of loop rotating heat pipe for cooling motorized spindle." *Applied Thermal Engineering* 192 (2021): 116927. https://doi.org/10.1016/j.applthermaleng.2021.116927
[38] Zhang, Yuwen, and Amir Faghri. "Advances and unsolved issues in pulsating heat pipes." *Heat transfer engineering* 29, no. 1 (2008): 20-44. https://doi.org/10.1080/01457630701677114
[39] Wang, Jiansheng, He Ma, and Qiang Zhu. "Effects of the Evaporator and Condenser Length on the Performance of Pulsating Heat Pipes." *Applied Thermal Engineering* 91 (2015). https://doi.org/10.1016/j.applthermaleng.2015.08.106
[40] Xu, J. L., Y. X. Li, and T. N. Wong. "High speed flow visualization of a closed loop pulsating heat pipe." *International Journal of Heat and Mass Transfer* 48, no. 16 (2005): 3338-3351. https://doi.org/10.1016/j.ijheatmasstransfer.2005.02.034
[41] Ling, Yun-Zhi, Zhang, Xiao-Song, and Wang, Xiaolin. "Study of Flow Characteristics of an Oscillating Heat Pipe." *Applied Thermal Engineering* 160 (2019): 113995. https://doi.org/10.1016/j.applthermaleng.2019.113995
[42] Fritz, Willy. "Numerical simulation of the peculiar subsonic flow-field about the VFE-2 delta wing with rounded leading edge." *Aerospace Science and Technology* 24, no. 1 (2013): 45-55. https://doi.org/10.1016/j.ast.2012.02.006
[43] Shimokusu, Trevor J., Drolen, Bruce, Wilson, Corey, Didion, Jeffrey, and Wehmeyer, Geoff. "Strain Gauge Measurements of an Oscillating Heat Pipe from Startup to Stable Operation." *Applied Thermal Engineering* 233 (2023): 121118. https://doi.org/10.1016/j.applthermaleng.2023.121118
[44] Qian, Ning, Marco Marengo, Jiajia Chen, Yucan Fu, Jingzhou Zhang, and Jiuhua Xu. "Heat Transfer and Temperature Characteristics of Single-Loop Oscillating Heat Pipe under Axial-Rotation Conditions." *International Journal of Heat and Mass Transfer* 197(2022): 123308. https://doi.org/10.1016/j.ijheatmasstransfer.2022.123308
[45] E, Jiaqiang, Zhao, Xiaohuan, Deng, Yuanwang, and Zhu, Hao. "Pressure Distribution and Flow Characteristics of Closed Oscillating Heat Pipe during the Starting Process at Different Vacuum Degrees." Applied Thermal Engineering 93 (2016): 166-173. https://doi.org/10.1016/j.applthermaleng.2015.09.060
[46] Nerella, Santhi Sree, Panitapu, Bhramara, and Nakka, Sudheer V V S. "Fluid Flow Analysis in a Closed Loop Pulsating Heat Pipe - Simulation Study." *Materials Today: Proceedings* 65 (2022): 3558–3566. https://doi.org/10.1016/j.matpr.2022.06.148
[47] Abdelnabi, Mohamed, Ewing, Dan, and Ching, Chan Y. "Onset and Performance of a Two Layer Oscillating Heat Pipe in a Heat Spreader." *Thermal Science and Engineering Progress* 46 (2023): 102217. https://doi.org/10.1016/j.tsep.2023.102217
[48] Pouryoussefi, Sam Mohamad Hassan, and Sohrab Gholamhosein Pouryoussefi. "Numerical study of flow visualization and thermal performance for pulsating heat pipes." *Journal of Aerospace Science and Technology* 15, no. 2 (2022): 17-24. https://doi.org/10.22034/jast.2022.346070.1119